Journal of Corrosion and Materials
www.corromat.com

J. Corros. Mater. (2024) 3(1), 51–66.

Co_3O_4 Nanoparticle Epoxy Coatings on Carbon Steel in Chloride Medium: Hydro-Dielectric Control, Specific Resistance, and Damage Retention

David R. Yarkony[1,*]

[1] *Department of Chemistry, Johns Hopkins University, Baltimore, Maryland 21218, USA*

[*] Corresponding author: yarkony@jhu.edu

(Received: 1 March 2024. Received in revised form: 18 May 2024. Accepted: 6 June 2024. Published online: 30 June 2024.)

Abstract

The efficacy of epoxy-based coatings for protecting carbon steel is normally assessed based on isolated measurements, yet corrosion usually results from the coupling of water absorption, electrolytic diffusion, localized mechanical degradation, and under-the-film corrosion processes. An attempt is made here to investigate the effect of adding 2.5 wt% Co_3O_4 nanoparticles as a coupled approach to modifying film formation, intrinsic barrier capability, the water-induced dielectric availability of the coating film, and mechanical protection against failure. The coating system included carbon-steel metal having 0.242 wt% C, 0.043 wt% P, 0.301 wt% Si, 0.030 wt% S, and 0.482 wt% Mn, coated by pure or Co_3O_4-based epoxy resins cured with a poly-amidoamine hardener in a ratio of 2:1 for epoxy to hardener. The oxide nanostructure had characteristics of spinel crystallinity, a mean crystallite size of 13.20 nm, a zeta potential of -20.5 mV, BET surface area of 92.4 $m^2\ g^{-1}$, and mean pore diameter of 19.8 nm. Soaking for seven days in 3.5 wt% NaCl solution at 298 K caused the coating film resistance to rise from 15.3 to 84.4 $M\Omega\ cm^2$, and the capacitance value to drop from 1.6×10^{-8} to 0.78×10^{-9} F cm^{-2}. Adjusting for differences in dry film thickness raised the contribution to resistance of each micrometre of the epoxy layer 3.96 times, and suppressed the normalized coating capacitance term 14.72 times. The increase in hardness, scratch resistance, and impact resistance of the coating were 3.53, 1.59, and 1.86, respectively, for a combined retention factor of 2.19. Coupled barrier and damage resistance resulted in an overall retention coefficient of 4.08, indicating that hydro-dielectric stability of the coating film is the critical enhancement mechanism, along with intrinsic resistivity and enhanced mechanical protection against damage. In summary, the protective function of the coating is due to its ability to limit the formation of water-accessible channels and make it more difficult for electrolyte to infiltrate via such channels.

Keywords: Co_3O_4 nanoparticles; epoxy nanocomposite; carbon steel; electrochemical impedance spectroscopy; coating capacitance; chloride corrosion; mechanical retention; salt spray.

1. Introduction

Carbon steel remains widely used in marine construction work, shipbuilding, tanks, bridges, pipelines, plant machinery, and transportation structures because carbon steel possesses many desirable qualities related to availability, welding and forming abilities, strength properties, and economic factors. The main drawback of carbon steel is associated with electrochemical rather than mechanical behavior. When in contact with solutions containing chlorides, local areas of the highly ferric matrix become susceptible to localized anodic dissolution whenever oxygenated solutions with aggressive ions contact the metal surface. Electrical and electrochemical measurements provide an early basis for linking coating response with corrosion at the metal–organic interface [1]. Paint-protection studies show that coating performance depends on delaying water, oxygen, and ion access to the substrate [2]. Organic-coating science also emphasizes adhesion, defect propagation, and barrier continuity as central durability requirements [3]. Modern anticorrosive-coating reviews confirm that ionic barrier action, dielectric behavior, water transport, oxygen transport, and adhesion must be interpreted together [4].

Epoxy resins have an important place among the anticorrosive coatings due to their strong adhesion to steel, chemical resistance, and relatively dense cross-linking density. Though the network formed by curing the epoxy resin is able to limit initial penetration of the electrolyte rich with chlorides, it does not behave like an ideal dielectric wall. Local free volume, poor wetting of the substrate, contraction of the cured film, disparity of surface roughness, microvoids, clusters of absorbed water molecules, interfaces between the pigments or fillers, and cracks due to damage may lead to formation of discontinuous or even continuous pathways. Corrosion can take place underneath the coating once these pathways provide a route from the solution through to the steel–coating interface [5]. Impedance investigation of underpaint corrosion shows that this buried interface can become electrochemically active even when the coating surface still appears continuous [6]. Capacitance measurements also show that water uptake and swelling can disturb the ideal dielectric interpretation of an organic coating [7]. This complex interfacial space can promote additional corrosion due to interfacial alkalisation, corrosion product deposition, osmotic blistering, coating expansion, and reduction of adhesion. As a result, a coating which

successfully resists corrosion at the early stage of immersion can lose its integrity later on due to accumulation of water, development of polar domain, and destruction by scratching or impact load.

Among the tools used to examine the performance of a protective coating, electrochemical impedance spectroscopy can be singled out since it allows examining conductivity, dielectric behaviour, porosity, and interfacial reaction without damaging the coating intentionally. Higher resistance means the presence of less ions, and smaller capacitance indicates less water accumulation and stable dielectric response. EIS has been widely used for studying corrosion protection by polymer coatings [8]. The problem with this technique arises when comparing coatings different in dry-film thickness, since higher film resistance can be explained not only by reduced conductive properties of the coating itself, but also by increased film thickness. Thermal-cycling and accelerated-evaluation studies show that coating resistance must be read in relation to exposure and film condition [9]. Functional and smart-coating reviews further stress that barrier, active, and structural effects should not be merged into one unexplained improvement [10]. Correspondingly, lower capacitance results not only from reduced water content, but also from increased dielectric film thickness. This problem is relevant also in the case of a filler-based coating, in which introduction of filler may change the viscosity, leveling behavior, thickness, local free volume, dielectric properties, and hardness of the coating.

However, such an approach of enhancing multi-property performance via nanoparticle addition relies on modifying the internal film structure to create barriers, to induce tortuosity, to fill voids, to reduce polymer mobility, and to resist external mechanical deformation. The efficacy of these mechanisms depends strongly on the degree of nanoparticle dispersion, which could lead to reinforcement and disruption of transport routes if uniform, but would otherwise be associated with stress concentrations, heterogeneous curing, and permeation pathways. Nanoparticle-filled epoxy coatings can improve anticorrosion and mechanical behavior when the particles are well dispersed [11]. Polymer-nanoparticle composite studies show that synthesis route and dispersion state strongly affect final material behavior [12]. Epoxy–clay nanocomposite research confirms that filler addition may improve corrosion resistance through altered transport paths [13]. Carbon-nanotube epoxy coatings also demonstrate that filler content can influence adhesion, wear, and corrosion response at the same time [14]. Depending on the properties of a given nanofiller, its dispersion characteristics, surface functionalization, loading ratio, binder interaction, and stiffness-toughness trade-offs, the same material might have either reinforcing or degrading effects on a polymer film.

In the present study, we are interested in Co_3O_4 nanoparticles as a potential filler of an epoxy resin. As a spinel oxide, cobalt oxide possesses some desirable traits of nanomaterials including high crystallinity, a large surface area, chemical inertness, and surface functionalization opportunities. However, contrary to the zinc pigment used in sacrificial corrosion protection systems, cobalt oxide nanoparticles cannot contribute as sacrificial material because of their poor conductivity. Instead, the main effect of such nanoparticles in an epoxy polymer matrix must consist in modification of the polymer network. Such modifications include the creation of tortuous transport paths, an increase in the polymer-filler interface area, and resistance to local deformations. Nanoparticles could also affect the curing process at a molecular level and polar domain distribution. When dispersing the nanoparticles adequately, the resulting nanocomposite becomes less permeable to chloride-containing water, as well as mechanically more resistant to damage propagation. On the other hand, agglomerated particles can form weak spots. The key point of interest here is whether a cobalt-oxide-filled epoxy provides increased performance because of film thickness, resistance per unit thickness, water-induced dielectric suppression, mechanical retention, or a combination of all of these effects.

This paper analyzes the effects of Co_3O_4 nanoparticle epoxy coatings on carbon steel in terms of a thickness-corrected hydro-dielectric and damage-retention assessment. The system of coatings analyzed in [15] considers an epoxy coating without modification to an epoxy coating with 2.5 wt% Co_3O_4. The measured properties are as follows: dry-film thickness, coating resistance, coating capacitance, nanoindentation hardness, scratch hardness, impact resistance, and response to 168 h of salt spray exposure. These properties are considered together in a single protection issue rather than separately as electrochemical and mechanical measurements.

Taking into consideration the increased thickness of the film made possible by the Co_3O_4 nanoparticle-modified epoxy, the coating is evaluated with the question of which performance path governs the improvement to carbon steel exposed to chloride. Resistance is assessed in terms of a per-thickness barrier term; capacitance is assessed in terms of a thickness-corrected hydro-dielectric term; and mechanical protection is considered in terms of a combined retention term based on hardness and impact data. Such an assessment does not introduce a new measurement process, nor does it rely on a single desirable reading to define protection. Rather, it considers whether a coating is less inherently conductive of ions, less subject to hydration-induced polarization, and less vulnerable to mechanically induced ingress routes. Such an analysis leads to identification of changes made to epoxy coating properties by addition of Co_3O_4 nanoparticles exposed to chlorides.

2. Materials and measured quantities

The material used in this study was a carbon steel with 0.242 wt% carbon, 0.043 wt% phosphorus, 0.301 wt% silicon, 0.030 wt% sulfur, 0.482 wt% manganese, and the rest iron. This particular alloy was chosen since chloride-related coating resistance to corrosion of carbon steels depends primarily on the continuous character of the epoxy film. The coating was formed using epoxy resin and poly-amidoamine hardener at a ratio of 2 parts epoxy per 1 part hardener by weight. Two types of coating were used: pure epoxy film denoted EP, and Co_3O_4 nanoparticles-modified epoxy film called Co_3O_4-EP. Since the focus of this study is a comparison of two materials rather than establishing the dependence of properties on loading concentration, the number of coating states under consideration is limited.

The oxide nanoparticles utilized in this study had a spinel crystalline structure, a mean crystallite size of 13.20 nm, a zeta potential value of -20.5 mV, a surface area of 92.4 m^2g^{-1}, and an average pore size of 19.8 nm. The zeta-potential value is relevant because particle surface charge is closely connected with colloidal stability and dispersion behaviour [16]. These parameters indicate that Co_3O_4 nanoparticles are able to influence the coating behavior due to the interface between the filler and the matrix. Namely, a particle with crystallite size in nanometers range can potentially interact with local free volumes of the polymer and contribute to tortuosity of the diffusion path. A negative surface charge reflects the existence of electrokinetic interactions in the dispersion state, while high surface area and mesopore size facilitate the interfacial effect of particles.

Figure 1 shows the morphology of the oxide nanoparticles and demonstrates visually the parameters described above. The image confirms the assumption that the filler interacts with the epoxy film at the nanometric level.

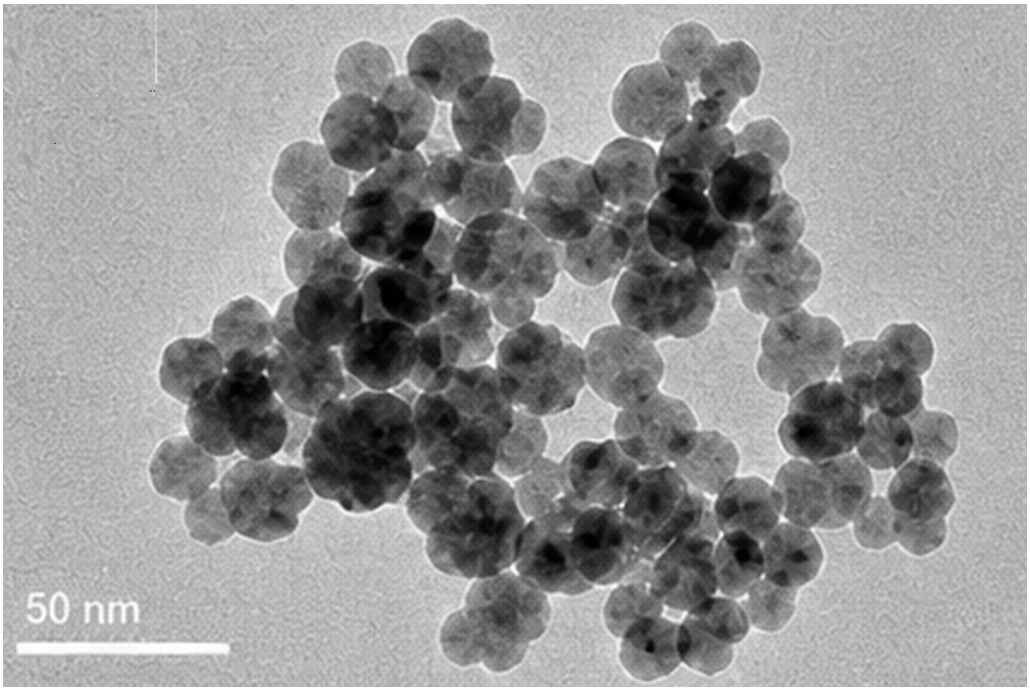

Figure 1: Co_3O_4 nanoparticle morphology.

Descriptor Summary in Figure 2 combines the measured numerical powder descriptors involved in the interpretation. The values of the crystallite size, zeta potential, BET specific surface, and pore-size suggest that the coating is formed due to the oxide-polymer interfacial contact, dispersion behavior, and physical interruption of the electrolyte pathway rather than due to the sacrificial metallic behavior.

Parameter	Value
Crystallite size (nm)	13.20
Zeta potential (mV)	−20.5
BET surface area (m^2 g^{-1})	92.4
Pore size (nm)	19.8

Figure 2: Nanoparticle descriptors measurements.

EIS parameters were considered for the samples that have been immersed for seven days into 3.5 wt% NaCl solution at 298 K. The area of the electrode covered by the coating was 30 mm x 10 mm. Dry-film thickness of the epoxy sample was 45.2 ± 3 μm, whereas that of the coated sample was 63 ± 4 μm. This disparity is sufficient for the further interpretation of EIS data because the absolute coating resistance and capacitance must account for the thickness difference. The ratio between the two films is 1.39. It means that, despite no consideration of the microstructural features, the oxide-containing coating provides longer pathway to the electrolyte.

Cross-sectional difference in Figure 3 shows the discrepancy in the thickness of the dry films, which is important to consider before discussing the EIS results. Although Co_3O_4-EP film is thicker, this difference will be accounted for by the normalized resistance.

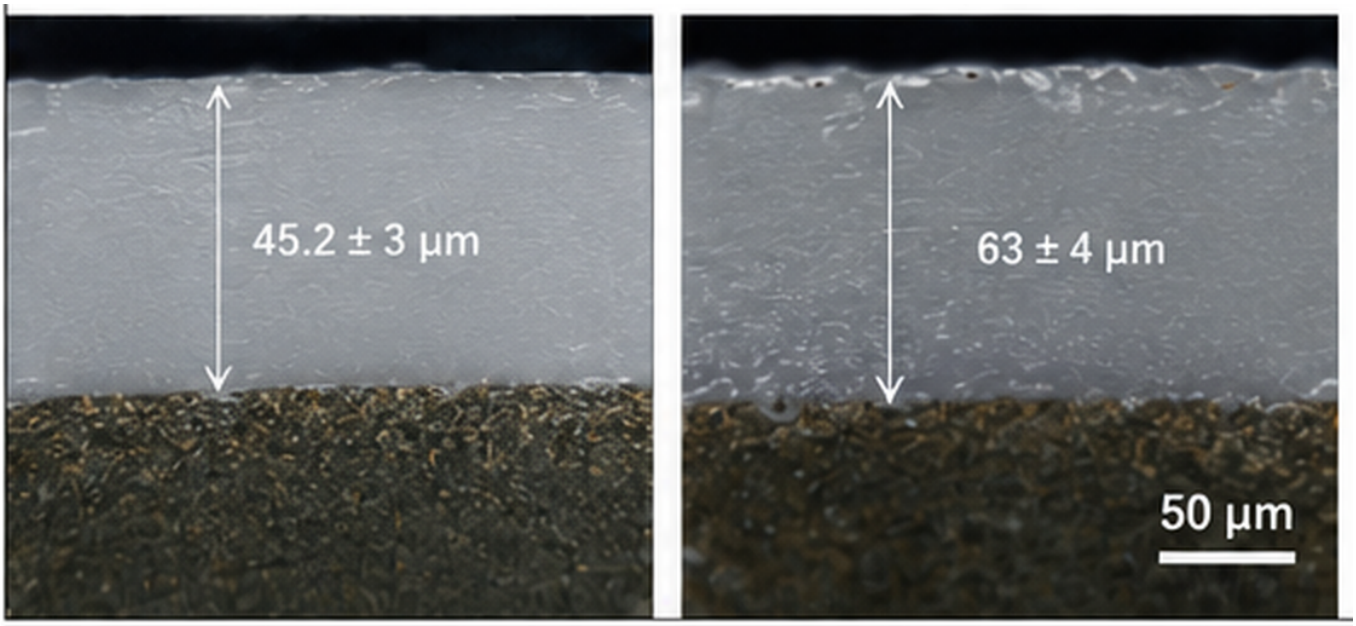

Figure 3: Dry-film-thickness comparison.

Parameters for coating resistance R_c and coating capacitance C_c were selected as key electrochemical response parameters. EP coating values were: $R_c = 15.3$ MΩ cm^2 and $C_c = 1.6 \times 10^{-8}$ F cm^{-2}. For the Co_3O_4-EP coating, the following values were obtained: $R_c = 84.4$ MΩ cm^2 and $C_c = 0.78 \times 10^{-9}$ F cm^{-2}. Direct ratio between the resistances is 5.52, while the ratio between suppression of the capacitance is 20.51. Although the ratio already demonstrates significant changes in protective properties, further discussion of the obtained values needs to take into account film thickness difference. One should consider resistance in terms of the unit of thickness, as well as adjust capacitance by thickness. Otherwise, higher capacitance may mean not improved structural properties, but only increase in the thickness of the dielectric layer due to moisture absorption.

Nanoindentation hardness, scratch hardness, and impact resistance were used to express mechanical strength of the coatings. Values for EP coating were: nanoindentation hardness - 0.126 GPa, scratch hardness – 5.6 GPa, and impact resistance – 42.2 kJ cm^{-2}. For the Co_3O_4-EP coating: nanoindentation hardness – 0.445 GPa, scratch hardness – 8.9 GPa, and impact resistance – 78.5 kJ cm^{-2}. All three measurements represent various routes of deformation of the films. Hardness during indentation is a result of material resistance to penetration, scratch hardness depends on the ability to resist lateral deformation and damage, and impact resistance demonstrates ability of the films to sustain high-rate deformation. This selection of parameters was made as underfilm corrosion of the coatings could start not only from existing pores but also due to mechanical damage to the film surface.

Table 1: Experimental coating values

Property	EP	Co_3O_4-EP
Dry-film thickness, δ (μm)	45.2 ± 3	63 ± 4
Coating resistance, R_c (MΩ cm^2)	15.3	84.4
Coating capacitance, C_c (F cm^{-2})	1.6×10^{-8}	0.78×10^{-9}
Nanoindentation hardness, H (GPa)	0.126	0.445
Scratch hardness, S (GPa)	5.6	8.9
Impact resistance, I (kJ cm^{-2})	42.2	78.5
Salt-spray exposure (h)	168	168

The results in Table 1 create an informative but concise coating history. On the electrochemical side, there is a clear trend of reduced dielectric response accessible by the electrolyte and enhanced impedance of charge transfer within the coating. From a mechanical standpoint, there is a clear enhancement in hardness and wear resistance across all measured modalities. The most telling aspect of the measured values is that there is a combination of higher dry-film thickness and enhanced electrochemical performance. A straight comparison would not be incorrect but incomplete as it might be difficult to disentangle the portion of the resistance increase caused by higher thickness. The following discussion takes those factors into account and then compares them with each other and with mechanical performance.

As opposed to visual corrosion observations, the present discussion uses a hydro-dielectric interpretation, which was used in classical as well as modern EIS literature. According to that work, water uptake was strongly associated with changes in capacitance [7]. Constant-phase and roughness effects may also complicate the conversion of EIS response into a single physical quantity [17]. Actual changes were therefore prone to deviations caused by non-uniform swelling, interface modification, porosity, and frequency dispersion. In line with that, the current analysis is done based on measured values to allow for a straightforward comparative evaluation. The aim here is not to provide an exact water volume fraction using only one parameter. Rather, the idea is to see if an oxide-filled coating prevents the manifestation of the dielectric response in question.

3. Barrier and Damage Retention with Thickness Correction

In the first computation, a particular resistance gain is introduced, denoted as G_R, which is based on the resistance contribution per micrometer of dry-film thickness:

$$G_R = \frac{R_{c,\mathrm{NP}}/\delta_{\mathrm{NP}}}{R_{c,\mathrm{EP}}/\delta_{\mathrm{EP}}}. \tag{1}$$

Here, $R_{c,\mathrm{NP}}$ and $R_{c,\mathrm{EP}}$ stand for the resistances of Co_3O_4-EP and EP coatings, respectively, whereas δ_{NP} and δ_{EP} are their dry-film thicknesses. The quantity introduced above determines whether the additional resistance provided by a micrometer of nanoparticle-coated film is larger than the same contribution by a micrometer of the original coating. Thus, it is possible to distinguish between the case where the barrier is improved structurally and the mere extension of transport path is observed.

The second term G_C is hydro-dielectric suppression gain and is defined as the product of capacitance and dry-film thickness normalized according to the formula below:

$$G_C = \frac{C_{c,\mathrm{EP}}\delta_{\mathrm{EP}}}{C_{c,\mathrm{NP}}\delta_{\mathrm{NP}}}. \tag{2}$$

In a perfect dielectric, capacitance is inversely proportional to thickness. The product of capacitance and thickness provides a rather conservative approach to evaluating the state of the dielectric. Hence, if G_C has a high value, then Co_3O_4-EP shows lower thickness correction of dielectric properties than the unmodified coating, indicating that its thickness-adjusted response is weaker in water-associated polar access or its internal structure is more stable.

Finally, an electrochemical barrier ratio can be represented through a combination of the aforementioned quantities via a multiplicative mean:

$$G_E = \left(G_R G_C\right)^{1/2}. \tag{3}$$

The multiplication mean is chosen since corrosion protection by an organic coating relies on ionic conductivity resistance as well as on prevention of water-related dielectric conductance. Very high values in either electrochemical variable cannot be allowed to compensate for low values of another. Such a choice allows constructing an electrochemical factor of interest while preserving the contributions from the two terms independently.

The mechanical retention factor, G_M, is composed of nanoindentation, scratch and impact hardnesses:

$$G_M = \left(\frac{H_{\mathrm{NP}}}{H_{\mathrm{EP}}}\frac{S_{\mathrm{NP}}}{S_{\mathrm{EP}}}\frac{I_{\mathrm{NP}}}{I_{\mathrm{EP}}}\right)^{1/3}. \tag{4}$$

It weights equally all deformation modes involved. A coating that exhibits very high hardness while being very susceptible to scratching or impact is given less merit for its hardness than it is actually due to. Taking the cube root allows being physically sensible since damage-assisted corrosion requires the coating to withstand more than one type of mechanical damage.

Finally, the coupling factor itself:

$$\Lambda = \left(G_E G_M\right)^{1/2}. \tag{5}$$

Λ can be interpreted as a comparative measure of performance of the Co_3O_4-EP system versus EP under current measurement conditions. It cannot serve as a prediction of any lifetime whatsoever and it cannot substitute any immersion, cyclic, adherence or cross-section tests. Its utility is to show whether the same changes to the coating formulation improve electrochemical barrier efficiency and damage-resistance in tandem.

The calculations have been intentionally kept relatively straightforward due to their utility in terms of physically interpretative ratios as opposed to arbitrary scores. Every ratio used here has a clear physical coating relevance: G_R measures intrinsic film resistance by thickness, G_C measures dielectric reduction by thickness correction, G_E measures equal electrochemical barrier performance, G_M measures balanced mechanical retention performance, and Λ measures joint resistance to electrolyte intrusion and damage-dependent pathway formation. It should be pointed out that this calculation technique is especially appropriate for organic nanocomposite coatings with EIS and mechanical values but no long-term coating data from field use.

4. Results and discussion

4.1 Nanoparticle descriptors and coating-structure plausibility

The descriptor characteristics of the cobalt oxide nanoparticles make up the material substrate for analysis of the coating performance. An average particle size of 13.20 nm means that the oxide phase particles can interact directly with free volume regions and cure and diffusion-related discontinuities in the epoxy network. It does not follow that any individual crystallite remains isolated within the final coating, but the material does have the right nanoscale properties to make a significant interface-related contribution. Regarding nanocomposite coating design, the best fillers are not only nanoscopic but also well-distributed so as to avoid voids and permeation-related weaknesses arising from agglomeration. The zeta potential of -20.5 mV could be of interest in view of its possible role in suspension stabilization before coating, although other factors affect coating structure including viscosity, mixing, and cure kinetics.

The surface area of BET, 92.4 $m^2\ g^{-1}$, is one of the critical characteristics here. High surface area increases the amount of epoxy that can be positioned around a polymer-oxide interface. Mobility of polymer chains in this interphase is not identical to bulk behavior of chains, and there might be additional contributions of the interphase into such parameters as local modulus, affinity to water, etc. The oxide becomes a barrier-forming component when it is successfully wetted by the epoxy. The pore size of 19.8 nm corresponds to a mesoporous surface structure. Although mesoporosity can favor physical interlocking of components, such pores may lead to creation of undesirable voids when their filling is insufficient. According to the obtained results on electrochemical properties of Co_3O_4-EP, it can be assumed that, at 2.5 wt%, oxide served as an agent that created tortuosity barriers but not defects.

4.2 Film build and resistance partition

Dry-film thickness grew from 45.2 μm in the case of EP up to 63 μm in the case of Co_3O_4-EP; hence, their ratio makes 1.39. Such significant difference should be taken into account before analyzing results of impedance measurements. The distance of migration for ions was increased independently of any changes in the polymer quality, which led to higher film resistance. However, in the studied record, absolute resistance was raised by 5.52 times, changing its value from 15.3 to 84.4 MΩ cm^2. Thus, the ratio between resistance increment and thickness increment is higher in this case. Resistance per unit film thickness makes 0.338 MΩ cm^2 μm^{-1} for EP and 1.340 MΩ cm^2 μm^{-1} for Co_3O_4-EP. The resulting specific resistance gain is 3.96.

This value is central to the interpretation because it demonstrates that the oxide-filled film is not simply a thicker form of the unmodified epoxy. Each micrometre of Co_3O_4-EP contributes almost four times the ionic resistance of each micrometre of EP. The most plausible explanation is that the oxide particles alter the internal connectivity of electrolyte-accessible pathways. In a homogeneous unmodified epoxy, chloride-bearing water can occupy free volume, microvoids, polar sites, and imperfectly cured regions. In a well-formed nanocomposite, dispersed rigid particles interrupt these local domains and force transport to follow a more tortuous route. Nanoparticle-modified epoxy studies support this mechanism when dispersion is controlled [11]. Epoxy–clay nanocomposite research provides a similar example of transport-path modification by filler addition [13]. ZnO-filled epoxy work also shows that oxide nanoparticles can modify thermal and mechanical behaviour of the cured coating [18].

The resistance partition also clarifies the limits of using a single EIS resistance value as a coating ranking. The raw resistance ratio of 5.52 is impressive, but it includes both film thickness and intrinsic barrier quality. The corrected gain of 3.96 is lower, more conservative, and scientifically more useful. It shows that about two features operate together: the coating is thicker and the material per unit thickness is more resistive. A coating engineer would interpret this as a favorable

outcome because the formulation improves the barrier even after the thickness advantage is removed. At the same time, the correction prevents overstatement by refusing to attribute the entire raw resistance increase to nanoparticle-induced densification.

The impedance graph plotted in Figure 4 gives us the electrochemical explanation for resistance breakdown. The larger response of the Co_3O_4-EP coating can be attributed to the limited ion transport through the coated surface after chlorine exposure; meanwhile, the next thickness adjustment breaks down the large dry-film build into two different responses.

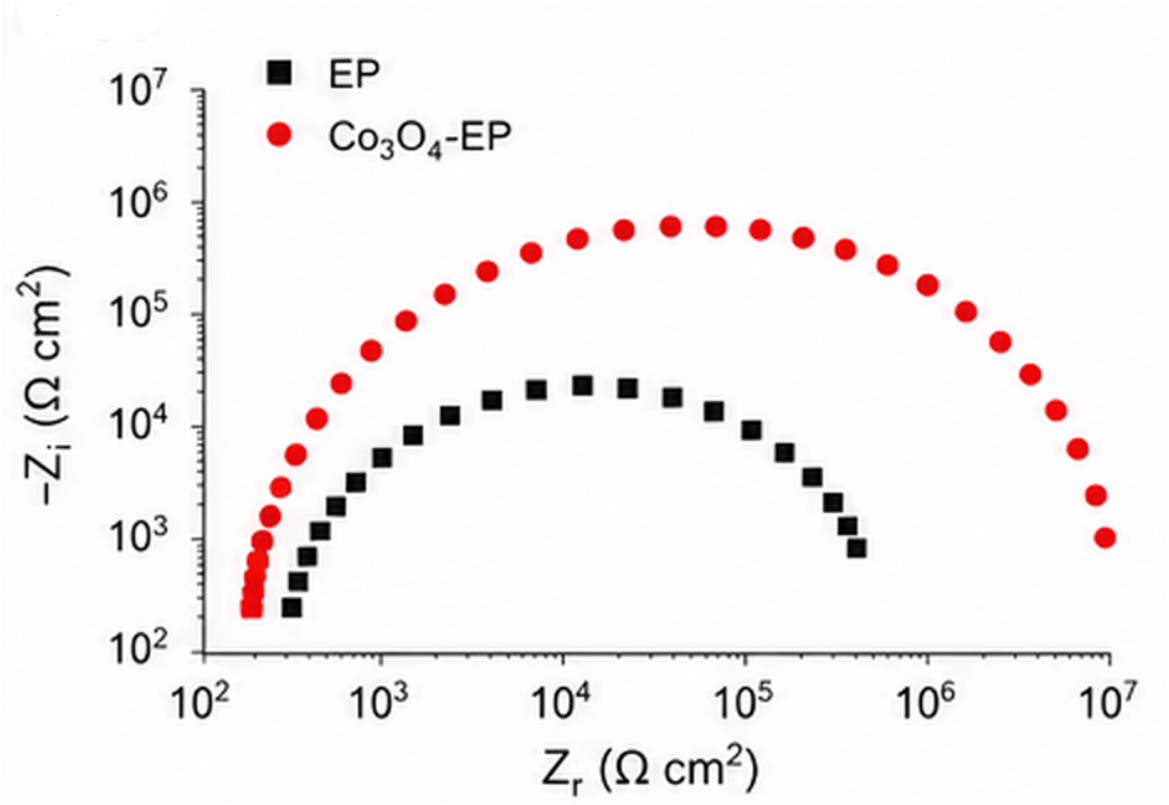

Figure 4: EIS response after chloride exposure.

4.2.1 Hydro-dielectric suppression

The capacitance response is even more telling than the resistance response. In terms of absolute coating capacitance, the reduction went from 1.6×10^{-8} F cm^{-2} for EP to 0.78×10^{-9} F cm^{-2} for Co_3O_4-EP. The direct suppression ratio is 20.51, showing that the oxide-loaded film shows significantly lower dielectric effects after chloride attack. The sensitivity of capacitance to changes in film thickness, dielectric constant, water content, and polar transport domains requires further adjustment of the ratio. The product of capacitance and thickness yields 7.23×10^{-7} F cm^{-1} for EP and 4.91×10^{-8} F cm^{-1} for Co_3O_4-EP. This gives hydro-dielectric suppression gain of 14.72.

The magnitude of this number affects the mechanistic explanation of the coating behavior. While the main impact of adding the oxide is a higher resistance, the most important factor is the hydro-dielectric suppression. Because the coating capacitance is an indicator of the dielectric properties and has been successfully used to monitor moisture absorption in wet coatings for decades, this large correction tells us that there are far less polar domains available to water molecules within the composite coating [7]. Resistance can be very high when the moisture content is still increasing due to isolation or partial isolation of water domains. In this case, the hydro-dielectric effect acquires significant corrosive importance, since the water penetrated into the epoxy film not only changes an electrical characteristic. Water provides a medium for ion migration, enables the development of local cathodic-anodic coupling after reaching the interface, and may lead to swelling effects leading to reduced adhesion. Thus, a coating with a lower value of the corrected capacitance is characterized by a lower probability of the presence of a continuous polarizing structure of the medium, providing effective electrochemical activation under the coating. Therefore, Co_3O_4-EP coating not only inhibits ion migration but also reduces the total volume of the accessible dielectric phase for ions. This conclusion is particularly relevant since, as a rule, underfilm corrosion starts earlier than coating breakdown and cannot be detected by visual observation methods at the initial stages of the study.

Multiplication of the resistance factor by the corrected capacitance gives $R_G = (3.96 \cdot 14.72)^{1/2} = 7.63$. In this way, the relative electrochemical gains due to the increase in both parameters are considered equally. In other words, the sum of normalized factors characterizes a high electrochemical barrier efficiency, since both parameters of the Co_3O_4-EP

coating exceed unity. Thus, a synergic effect can be seen between the parameters used in the estimation of electrochemical performance, confirming the internal consistency of the results.

The EIS parameters shown side by side in Figure 5 make it clear why resistance and capacitance should not be examined separately. The oxide-loaded coating exhibits a greater value of R_c, but a far smaller value of C_c, meaning that electrochemical optimization involves both ionic blocking and reduced water-related dielectric behavior.

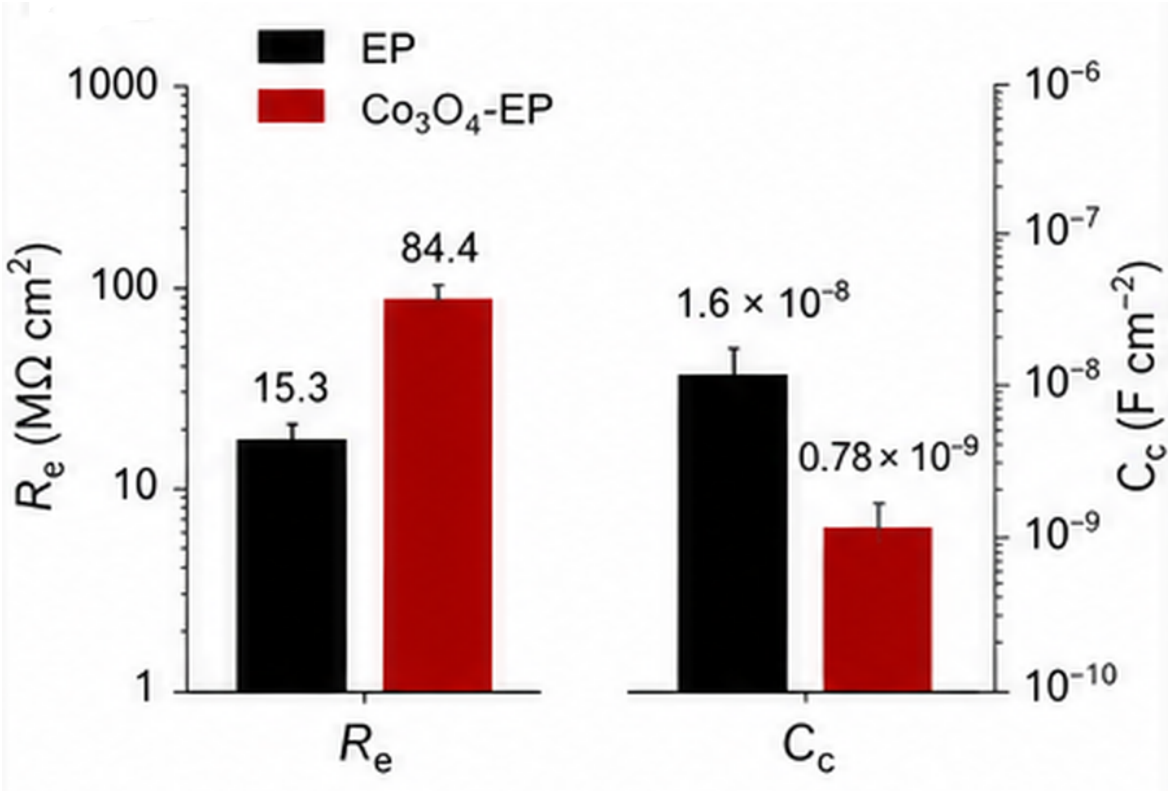

Figure 5: Resistance and capacitance values.

4.3 Mechanical Retention and Damage-assisted Ingress

In terms of the mechanical response, it is clear that the introduction of the oxide modifies more than the electrochemical aspect of the film formation process. Hardness under nanoindentation increased from 0.126 to 0.445 GPa, a gain ratio of 3.53. Hardness under scratch tests increased from 5.6 to 8.9 GPa, a gain ratio of 1.59. The impact resistance increased from 42.2 to 78.5 kJ cm^{-2}, a gain ratio of 1.86. These values indicate a general improvement in local penetration, lateral surface damage, and rapid deformation resistance. The mechanical retention factor for this film system is $G_M = (3.53 \times 1.59 \times 1.86)^{1/3} = 2.19$.

These mechanical data cannot be interpreted separately from the electrochemical data. In service environments containing chloride ions, the point at which electrolyte enters the metal structure depends on whether any damage occurs to the coating itself. Scratches, impact marks, and indentations can create a preferred path, despite the high impedance of the otherwise undamaged coating. Since the hardness under indentation tests has improved, this film type should offer enhanced resistance against local penetration into the coating film structure. Similarly, since scratch hardness has improved, this film type offers reduced risk of lateral gouging damage connecting external electrolyte to internal coating defects. Increased impact resistance implies that a film of this type will absorb rapid deformation before failure to maintain continuity of barrier. The product of factors 2.19 is smaller than the electrochemical barrier factor, but still sufficiently high to have practical meaning.

Asymmetry in the mechanical enhancement ratios is also telling. Hardness gain increases most significantly since additional rigidity due to the presence of a hard oxide phase leads to enhanced resistance against compressive stress. Scratch and impact gain are less dramatic due to the fact that these properties also depend on adhesion at the interface, continuous bonding of the polymer material, and toughness, along with increased ability to absorb impact energy. A coating that becomes too stiff is sometimes fragile, but the impact resistance gain shows that no simple fragility penalty is imposed by the 2.5 wt% oxide loading in the investigated system. Therefore, a proper description of this process is that of mechanical reinforcement rather than hardening.

Finally, the mechanical retention ratio also reinforces the proposed hydro-dielectric theory in some other way. A coating that is water resistant yet susceptible to cracking would still be susceptible to failure in service. Alternatively,

even if it possesses excellent mechanical properties as well as high water capacitance, such coating may still allow underfilm corrosion. Indeed, this oxide-containing composite coating demonstrates improvement of both aspects, but not equally well. Its maximum contribution is the suppression of dielectric effect, followed by improvement in resistance per unit thickness, and finally improved mechanical properties.

As is evident from the mechanical properties plot shown in Figure 6, the addition of oxide enhances all three measures of damage. Out of these, the largest improvement is seen in the hardness test conducted by the indentation technique, while scratching and impact tests serve as the indicators of its effectiveness in service.

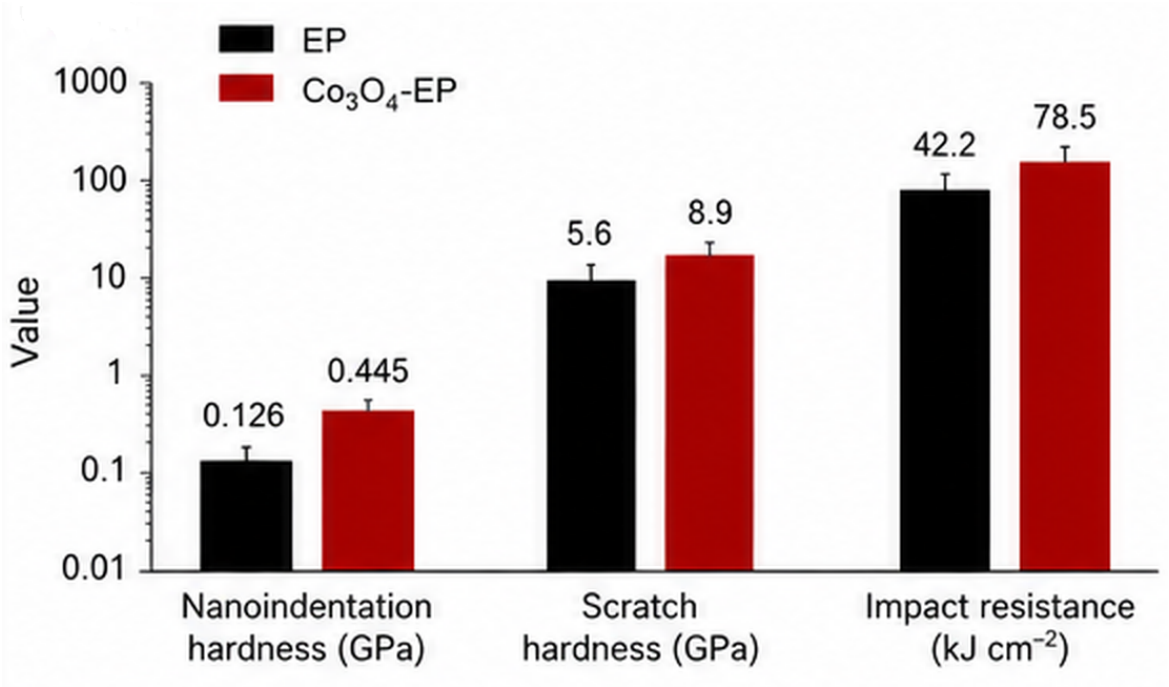

Figure 6: Mechanical property comparison.

Table 2: Derived protection terms

Derived term	Value
Film-thickness ratio, $\delta_{\mathrm{NP}}/\delta_{\mathrm{EP}}$	1.39
Direct resistance ratio, $R_{c,\mathrm{NP}}/R_{c,\mathrm{EP}}$	5.52
Specific resistance gain, G_R	3.96
Direct capacitance-suppression ratio, $C_{c,\mathrm{EP}}/C_{c,\mathrm{NP}}$	20.51
Hydro-dielectric suppression gain, G_C	14.72
Electrochemical barrier partition, G_E	7.63
Nanoindentation hardness gain	3.53
Scratch hardness gain	1.59
Impact resistance gain	1.86
Mechanical retention factor, G_M	2.19
Barrier-damage retention coefficient, Λ	4.08

The derived numbers from Table 2 indicate that the enhancement due to coatings is not determined by one particular quantity. The difference between the coating thickness ratio of 1.39 and the resistance increase of 3.96 demonstrates that the film thickness cannot account for the resistivity change. The hydro-dielectric inhibition factor of 14.72 is the highest of all corrected responses and can thus be taken as the major process involved. The mechanical holding power of 2.19 is smaller than the electrochemical barrier fraction but still significantly larger than unity. The last number 4.08 is smaller than the electrochemical factor since it includes the mechanical effect as well.

4.4 Relative hierarchy of the measured responses

Having an order among the numerical values for the corrected quantities is a great benefit since it will make us not consider the coating by only one overwhelming uncorrected quantity. So, the direct value of the capacitance ratio is the largest (20.51), whereas the direct value of the resistance ratio is relatively small (5.52). After correcting for the thickness effect, both ratios are quite large, yet the difference between them is greater. While resistance correction tests the intrinsic difficulty for ion

transfer through the film, the capacitance correction tests another characteristic – the presence of water-related dielectric properties after removing the thickness effect. Much higher G_C indicates that this nanocomposite efficiently decreases those internal characteristics that allow water to exist within the sample as a connected electrochemical substance.

It is essential to know which of those two corrections is more critical when ranking chloride service coatings. Initially, the coating will exhibit some resistance due to the non-conductive nature of pores, but water will be able to enter them anyway and get ready for future interfacial activities. Thus, capacitance is a better early detector of the coating hydration compared to the development of corrosion manifestations or even low-frequency resistance in a particular moment. When the capacitance is decreased by some amount and then the thickness correction is applied, the resulting ratio of G_C is about 3.7 larger than the ratio of G_R. Such a big difference suggests that the oxide phase influences the water-accessible dielectric volume of the sample more actively than the resistive volume. The practical implication, therefore, is that the presence of Co_3O_4 influences the formation of the coating at the interface in ways that prevent conditions from forming for broad electrolyte-coupled activity.

It is also worth paying particular attention to the mechanical hierarchy, since the indentation data represents the largest mechanical shift. However, it must be noted that scratch hardness and impact resistance are the two service criteria used to determine the usefulness or brittleness of the hardening process. In some cases, nanoparticle-containing polymers exhibit increased hardness with a loss of ductility and impact resistance. Such an effect would be undesirable for protective coating, as brittle fracturing creates rapid pathways for electrolyte. In the case of Co_3O_4-EP films, neither of these drawbacks appears, as scratch hardness and impact resistance are both higher in the treated sample. Therefore, despite being the smallest measured value among the mechanical properties, the factor of 2.19 is rather conservative and demonstrates that oxide loading promotes mechanical resistance beyond simple hardness gain.

Finally, the lowest value (coefficient of 4.08) must be considered relative to the hierarchy of parameters rather than treated in isolation. Being below 7.63, it reflects the relatively weak mechanical enhancement compared to electrochemical one. Such a reduction is useful in order to avoid overestimating the mechanical properties of the material. Indeed, while all other properties have demonstrated an improvement, electrical characteristics showed particularly impressive results. Therefore, the coating may be considered to be better, which implies dominance of the electrochemical stabilization with respect to mechanical consolidation. Nonetheless, the ratio in question remains significantly greater than one because each domain behaves positively. In other words, the nanocoating has a certain property hierarchy: dielectric stabilization is dominant, per-unit-thickness resistance suggests barrier function, and mechanical retention is compatible with defect resistance. This hierarchy is much more meaningful than a conclusion about the overall superiority of the sample since it indicates the primary driver behind the observed benefits.

4.5 Correlation between chloride transport and interfacial activation via electrolyte penetration

As mentioned above, one can develop a physical picture of how the electrolyte interacts with a coating layer of interest. In pristine epoxy films, there is no necessity for water molecules to arrange themselves in a chain. The process of cluster formation may begin with isolated molecules; polarized microdomains and free-volume regions that are partially or completely separated from each other may combine gradually during film immersion in an electrolyte. As the conductivity and dielectric constant increase because of this process, it becomes easier for chloride ions to migrate closer to the steel/coating boundary. Then, they have access to a chemically active zone where oxygen is reduced because it penetrates through the film.

Nanoparticles of Co_3O_4, in turn, appear to prevent this kind of development. First, the presence of these particles implies that water and ions must move around a rigid inclusion instead of freely permeating the polymer matrix. Second, the oxide surface may prevent the formation of such domains by either attaching some polymer segments directly to itself or rearranging the polarity of neighboring sites. The significant BET surface area makes the second mechanism more relevant since relatively few oxide nanoparticles provide a lot of contact points. The obtained capacitance data support this view since the dielectric response is lower than expected even when accounting for the thickness difference.

The high measured resistance reinforces this interpretation, since the actual transport paths that are present will also be less conductive than those found in the case of coatings without such behavior. This is due to the fact that, while water uptake and ion transport are related, they are not one and the same thing. A coating can possess a lower permeability to ions even if its water domains are continuous and it holds a lot of moisture internally, since this moisture might form isolated pockets and there may be obstacles to charge transport along the ionic paths within the coating. This is precisely what occurs with the Co_3O_4-EP coating: the ionic transport within it becomes extremely difficult due to the lack of conductive domains.

Mechanical retention thus provides the third control on interfacial activation. A scratch-resistant coating that is stable

under immersion but subject to scratching will fail by another failure mode since scratches allow the coating defect to develop faster than the diffusion-controlled process of transport through the coating. Increased scratch resistance and impact strength are evidence that oxide loading increases the material's ability to prevent defect propagation. However, it does not imply that damage cannot occur in the film. Rather, it decreases the likelihood of damage turning into a wide access channel through which electrolytes may flow. For chloride conditions, such inhibition becomes critical since corrosion in defects tends to propagate laterally below the coating.

4.6 Comparison with general trends for nanocomposite coatings

The results reported for Co_3O_4-EP correspond to those from other successful nanocomposite coating formulations in which improvements in barrier efficiency occur only with controlled dispersion, adhesion, and network compatibility. Previous research conducted with nanoparticle-reinforced silicone-epoxy coatings found that nanoparticle dispersion plays a critical role in improving the overall barrier quality of the cured binder film [11]. Exfoliation and dispersion become important factors that influence the effectiveness of clay-based epoxy coating systems [13]. On the other hand, carbon nanotubes have been effective in improving mechanical and barrier properties of coatings but also pose challenges related to dispersion and conductivity [14]. The obtained values are more characteristic of a passive tortuosity and interphase mechanism.

Finally, this coating system should be considered distinct from the class of smart coatings that use nanocontainers for inhibitor delivery or have inhibitor reservoirs triggered by interfacial pH change. The earlier search for alternatives to chromate-based protection shows why active inhibition has long been an important coating-design route [19]. Self-healing or active systems release inhibitors upon pH change at the interface and therefore require control of release rate, matrix compatibility, and reservoir depletion [20]. Functional smart-coating reviews similarly show that active corrosion protection depends on controlled inhibitor availability rather than on barrier thickening alone [10]. In contrast, the performance of Co_3O_4-EP cannot be attributed to any release process; it can be explained through the presence of the coating structure with reduced hydro-dielectric exposure, increased ionic resistance, and reinforced integrity. Thus, it becomes clear that it is a viable choice for coatings requiring passive protection and high mechanical resilience without any need for an inhibitor.

As seen above, this also answers the question of the impossibility of a universal ranking of fillers according to their performance. For example, the same filler might perform poorly in another epoxy system due to differences in compatibility, dispersion, curing conditions, and surface modification. It follows that the meaningful scientific conclusion to be drawn here is not a generic conclusion about the performance of Co_3O_4 versus other fillers. Instead, what needs to be concluded is a quantifiable signature of the coating system: 14.72-fold capacitance reduction, 3.96-fold resistance improvement, and 2.19-fold retention of mechanical properties. These rankings define the mechanism of operation of the coating and permit comparison between prospective coatings on a physical level.

4.7 Salt spray performance and defect-dependent protection

The 168 h salt spray exposure gives physical relevance to the calculated ranking. Although salt spray testing is not an ideal simulation of long-term marine immersion or field exposure cycles, it helps in identifying behaviors that are sensitive to defects. The plain epoxy showed more signs of corrosion near the defective area, while the Co_3O_4 epoxy revealed less corrosion around the defect site. This observed outcome correlates with the rankings, as the oxide-modified coating impedes water-induced dielectric mechanisms, exhibits greater electrical resistivity with respect to the thickness and offers better mechanical strength.

The scratched coatings comparison shown in Figure 7 demonstrates the defect-dependent ranking. The bare epoxy shows increased signs of corrosion near the crossing scratch, whereas the Co_3O_4-EP coating has less affected areas around the defect.

The failure mechanism is important because coatings hardly ever fail simultaneously. Even a small flaw in the coating could lead to formation of an anode in the region. Meanwhile, the rest of the surface covered with the coating could become a cathode where reduction of oxygen could take place, provided that there is enough electrolyte and oxygen to do so. Generation of hydroxides at cathodic spots could lead to increased pH levels, causing degradation at the interface, and eventually blisters. Ferrous ions generated at anodic locations would react with oxygen and hydroxides, forming corrosion products that would exert stress on the coating. The anodic and cathodic reactions are illustrated below.

$$\mathrm{Fe} \rightarrow \mathrm{Fe}^{2+} + 2e^{-}, \tag{6}$$

$$\mathrm{O_2} + 2\mathrm{H_2O} + 4e^{-} \rightarrow 4\mathrm{OH}^{-}. \tag{7}$$

This illustrates how the two characteristics should go hand in hand because both the electrochemical reaction needs paths for ions, water, and oxygen, and the mechanical damage can open up paths through the oxide layer.

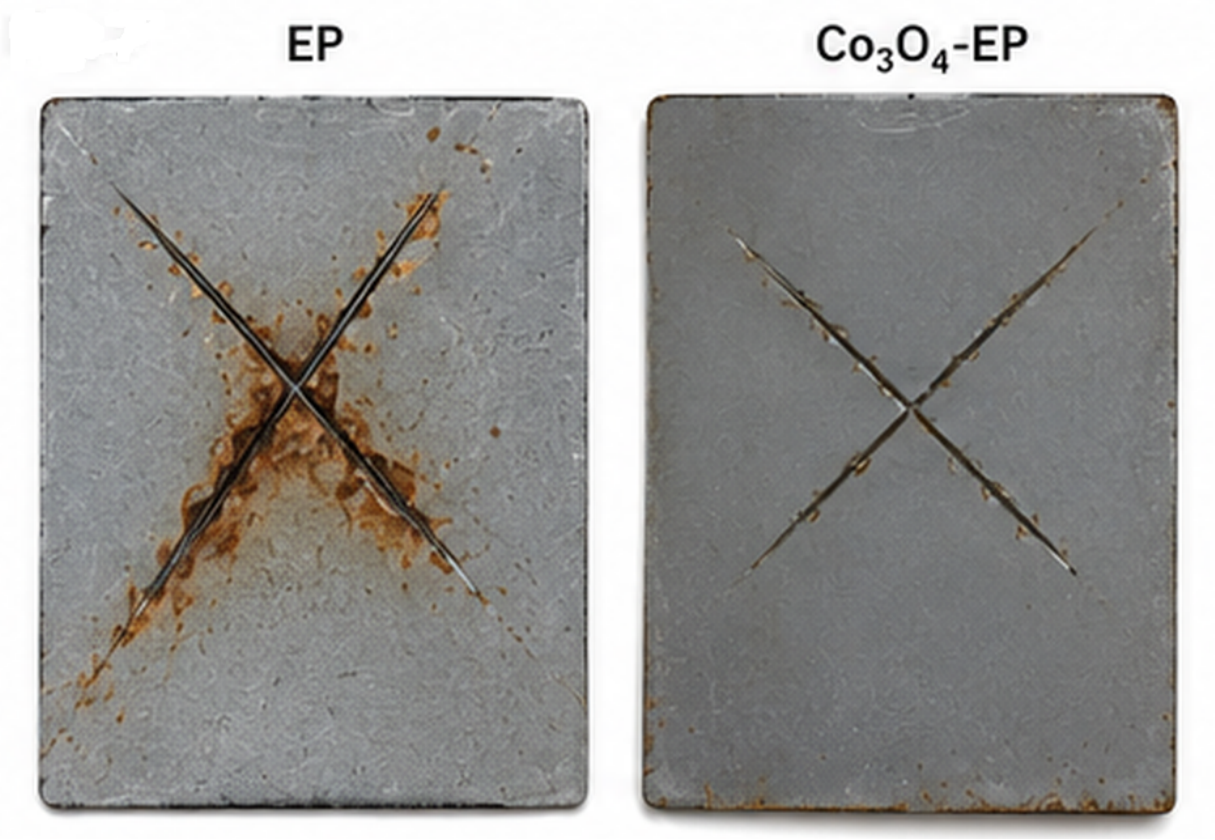

Figure 7: Defective coating surfaces after salt spray testing.

The lesser visible damage around the Co_3O_4-EP defect supports an electrocoat that restricts electrolyte flow and lateral growth of any underfilm attack. It seems like the low correction to capacitance indicates fewer places through which water can get through; the high correction to resistance indicates that there is greater resistance for any ion migration; and the mechanical retention factor indicates that there is a lesser probability of expansion of the damaged area. The three aspects above contribute to delaying the establishment of a continuous underfilm cell. In other words, it appears that the oxide-layered film is less conducive to spreading damage than its counterpart.

The surface picture below (Figure 8) takes on a defect-focused approach to underfilm damage along the damaged line. The stronger discoloration and accumulation of corrosion products around the EP defect support the low resistance, high capacitance, and poor mechanical retention of the film.

The salt-spray experiment also serves as a cautionary reminder that reliance on EIS with intact films alone should be limited. While a high impedance suggests good initial properties as a barrier layer, defects may cause a transition from bulk transport to lateral transport in the film/metal interface. Mechanical tests will assist in identifying how well an initially robust film maintains its barrier properties if it becomes scratched or impacted. In the present case, the salt-spray observations are not merely a standalone visual observation. Instead, they represent the practical aspect of the same testing approach noted earlier through the corrected EIS and mechanical calculations.

In contrast to the earlier exposure sequence, Figure 9 provides the visual interpretation of the chloride-induced damage of the coatings as a function of time. The quantified constant presented here still corresponds to the 168 h value in Table 1. However, the visual sequence clearly illustrates the same trend: the EP shows higher corrosion than the Co_3O_4-EP.

4.7.1 Mechanistic synthesis

A three-stage mechanism can be proposed for the protective properties of Co_3O_4-EP. The first stage is the obstruction of diffusion paths. The presence of oxide particles of nanoscale dimension in the cured epoxy film makes the diffusion path more complicated, making it necessary for the ions to follow a more meandering trajectory before arriving at the steel interface. This explains the 3.96-fold increase in specific resistance. The second stage is the reduction of hydro-dielectric volume. The substantial decrease in the relative capacitance suggests that there are fewer connected dielectric zones or polar areas, making the film less accessible to water. This stage is captured by the 14.72-fold increase in capacitance-dependent performance. The third stage is the increased resistance to damage formation. The higher values of the indenting force, scratching force, and impact energy suggest the reduced likelihood of damage to occur and become an electrolyte passage.

The effectiveness of each of these mechanisms stems from the mutual reinforcement of the three stages rather than their

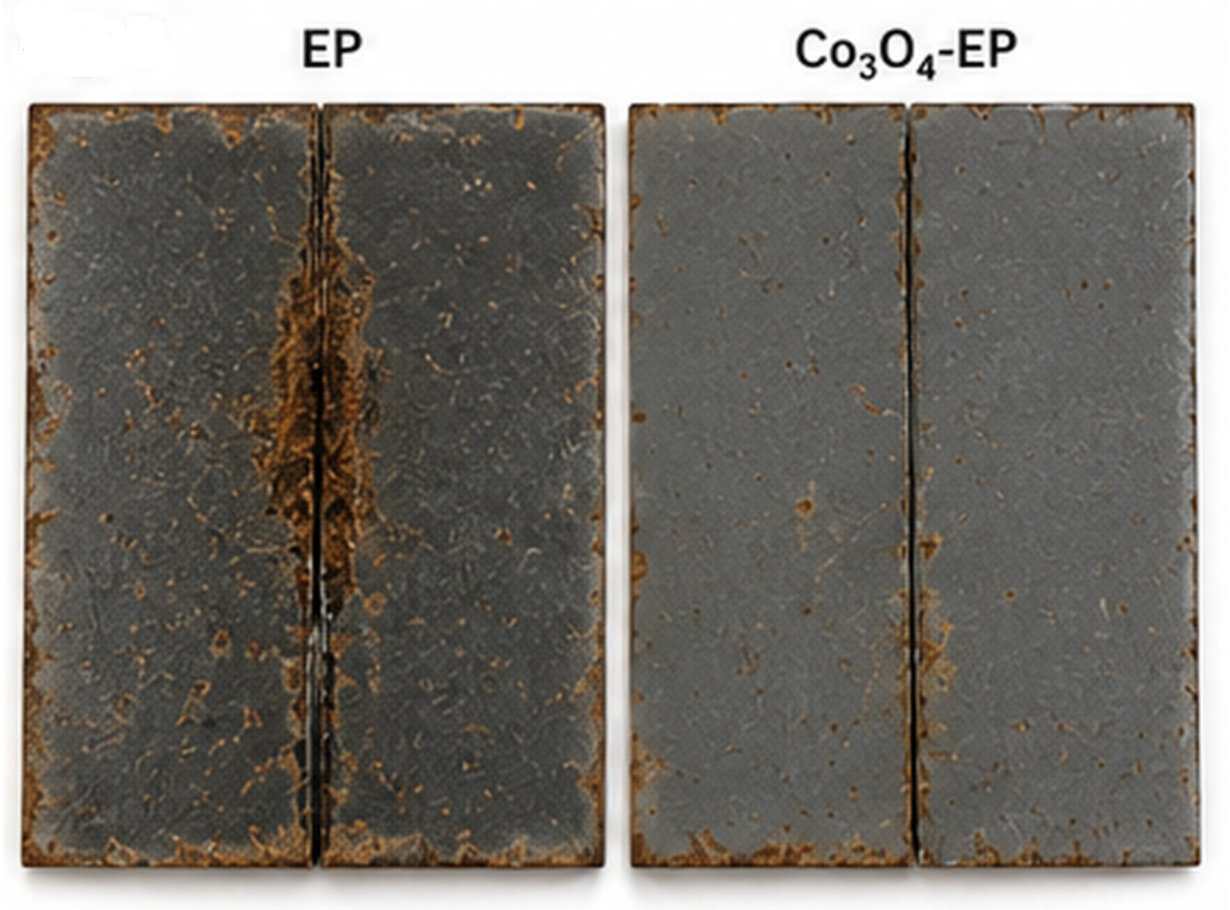

Figure 8: Defect-centered chloride attack.

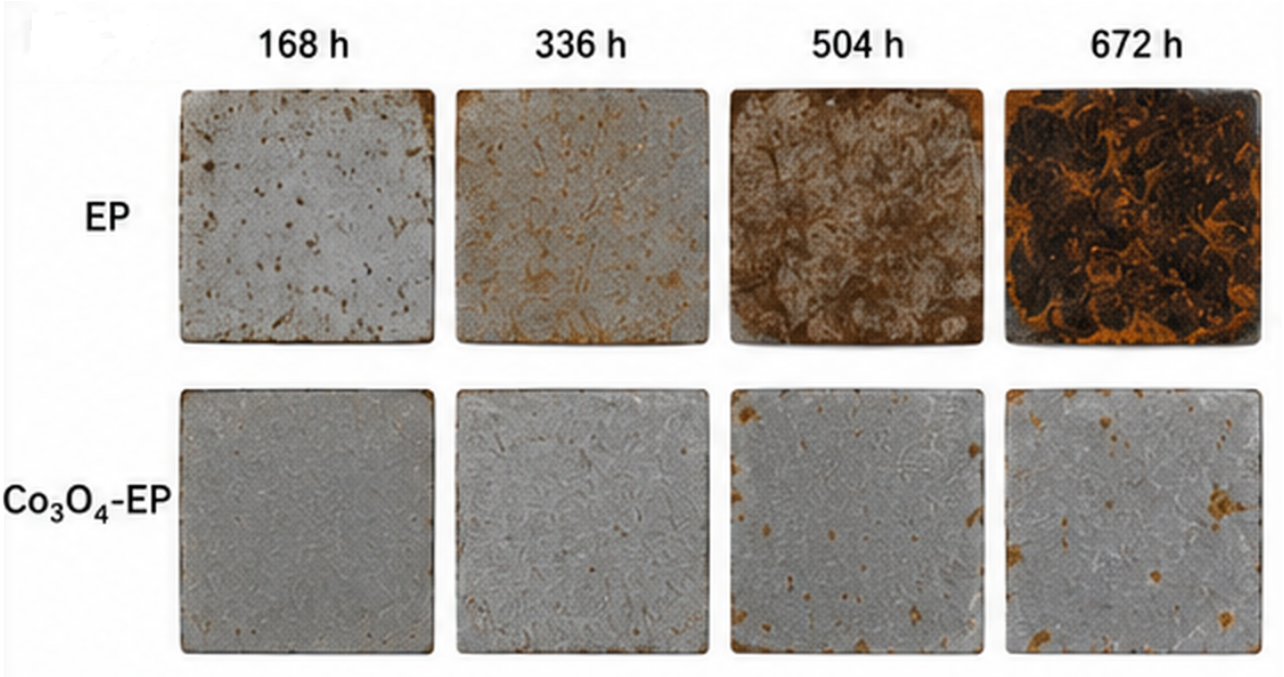

Figure 9: Chloride-exposure appearance sequence.

independence. Obstructing a path is valuable only when the material is also capable of storing less water; this makes the first two stages reinforcing one another. Being resistant to mechanical action is valuable only if electrolytes are not easily able to access the coating through other pathways, hence making the second and third stages complementary. Resisting damage is valuable only when it does not grow due to other damage; this makes the third stage dependent on the second. The retention factor of 4.08 accounts for this interdependence; despite being lower than the electrochemical barrier partition because of the smaller mechanical gains, it is still substantially above unity.

The preponderance of hydro-dielectric suppression in the observed effects separates the current coating from those where improvements arise mainly due to mechanical hardening or film thickness. In the former case, a change in thickness by one micrometre would have increased resistance proportionately, and capacitance correction would have mitigated the positive difference further. In the latter case, increase in the indentation hardness might have occurred without any notable effect on the capacitance change. The current data exhibits the opposite trend, which suggests that the main underlying process involves reduction of dielectric constant and its mechanical consolidation through resistance.

It can be said that the results obtained fit into the general context of research of coatings based on nanocomposites. Many materials were used for improving coating properties, such as clay platelets, silica nanoparticles, carbon nanotubes, graphene derivatives, porous coordination fillers and encapsulating inhibitors. Nanocontainer-based coatings can work through damage-triggered inhibitor release [20]. Clay-epoxy nanocomposites can improve barrier properties by changing diffusion pathways [13]. Smart-coating reviews show that several active and passive mechanisms may operate in different systems [10]. Graphene-based hollow-sphere coatings illustrate a dual active/barrier route through inhibitor nanoreservoirs [21]. For instance, platelet fillers may form a long diffusion barrier if exfoliated and oriented. Similarly, spherical oxide particles may fill the free volume of cured binder. On the other hand, nanocarriers may serve for effective release of active corrosion inhibitors, although they pose more compatibility problems.

4.8 Implications of design and limits of interpretation

The calculated value confirms the utility of the 2.5 wt% Co_3O_4 additive as multifunctional in the epoxy coating being considered; however, this does not mean that a higher amount would be better. The nanoparticle content has an optimal range, beyond which additional viscosity, contact, agglomeration, poor wetting, and interference with cure may lead to defects that reduce the advantages of tortuosity and reinforcement. Given the large G_C, future efforts in formulating the composite should consider optimizing dielectric and dispersing properties before adding more filler.

It may seem odd that Λ is dependent on the balance of properties. In other words, if a coating is thickened without improving its resistivity, it will have a smaller value of G_R. If it is hardened without reducing its hygroscopicity, it will have a smaller value of G_C, and thus a smaller overall coefficient. Similarly, a good EIS response along with poor mechanical behavior leads to a lower score. Consequently, this coefficient is appropriate for comparing polymeric nanocomposites where there is available information on EIS and mechanics. Moreover, it rewards full disclosure since thickness, capacitance, resistance, and mechanical parameters need to be determined simultaneously.

Limitations are no less critical. They are based on the values obtained under a certain exposure condition: 7 days of immersion in 3.5 wt% NaCl solution at 298 K in the case of EIS and 168 h salt spray exposure in the case of accelerated chloride challenge. The coating performance could vary with longer immersion time, cyclic wet-dry testing, UV aging, thermal cycling, or detachment. The coefficient doesn't include such tests as pull-off adhesion test, cross-hatch adhesion test, mass gain of water uptake, contact angle change, cross-sectional microscopy or analysis of the interfacial chemistry. All these tests will add more information concerning the coating mechanism. In addition, implementation of a time-dependent approach, where G_R, G_C, G_M, and Λ are calculated based on the results from several immersion intervals will be extremely helpful since durable coatings must keep their protective properties.

Neither the values nor the analysis resolves the exact spatial distribution of the Co_3O_4 particles within the polymer matrix. This is clear from the values of descriptors, and although the particles interrupt transport pathways, this assumption can be proven only with the help of microscopy or scattering technique. This interpretation of the mechanism is confirmed by the EIS and mechanical properties, but the full proof of the mechanism requires cross-sectional imaging and mapping for all filler loadings. These limitations don't diminish the gained results but outline necessary experiments for building the structure-performance correlation.

5. Conclusions

From the data presented above, we can determine if the improved protective efficiency of the oxide-modified coating is caused primarily by its thickness increase, resistance enhancement, hydro-dielectric characteristics, mechanical properties,

or their combination. According to the evaluation results, the enhanced performance of a 2.5 wt% Co_3O_4 nanoparticle-containing epoxy coating applied on carbon steel is caused primarily by hydro-dielectric stabilization, while resistance per unit thickness and mechanical damage resistance are the supporting effects. Although the dry film thickness increases 1.39 times, the resistance per unit thickness rises 3.96 times, which indicates that the oxide-containing layer is more resistant to ionic transport than an oxide-free epoxy coating.

The highest correction is associated with the 14.72-fold decrease in the thickness-correction factor for the capacitance term. From this data, it follows that the Co_3O_4-filled epoxy coating becomes less susceptible to the formation of dielectric-polar water regions after immersion in chloride solution. It is well known that water ingress is directly associated with the initiation of under-film corrosion; therefore, such changes are a clear indicator of oxide influence on internal coating barrier characteristics. The electrochemical barrier partition of 7.63 can be considered as an additional confirmation of this phenomenon based on the combined effect of resistance and capacitance.

From the mechanical values, it is evident that the oxide-coated epoxy film has become more durable due to 3.53-fold increase in hardness and 1.59-fold increase in scratch hardness and 1.86-fold increase in impact resistance leading to 2.19-fold mechanical retention improvement. Mechanical damage is an inevitable aspect of the use of coatings in real-world applications. Impact-resistance evaluation should remain connected with the relevant coating-damage testing practice [22]. Therefore, such improvements, although not as high as in the case of hydro-dielectric properties, still have great value as electrolyte-access creation mechanisms during coating usage in the chloride environment. Salt-spray exposure provides an accelerated chloride environment for checking visible corrosion resistance [23]. The results obtained from the salt spray test prove this conclusion.

The total barrier-damage retention coefficient of 4.08 allows providing a comprehensive answer to the question regarding the improved performance of the oxide-modified epoxy coating. Thus, Co_3O_4 nanoparticles increase the performance of epoxy coating primarily due to its dielectric nature in which water-accessable polar pathways become highly restricted while improving resistance and mechanical properties. Therefore, the barrier properties of such coatings become more durable and less prone to damaging effects of external factors.

Availability of numerical values

All numerical values used for calculation are listed in the tables and equations of this manuscript. Application of the calculations requires measurements of coating thickness, resistance, capacitance parameters derived from EIS tests, nanoindentation hardness, scratch hardness, impact resistance, and accelerated chloride exposure observation under similar conditions. Surface-treatment and coating-adhesion data should also remain traceable to the appropriate testing reference when such evidence is used in coating comparison [24].

Conflict of interest

The author declares no conflict of interest.

References

[1] Leidheiser Jr, H. (1979). Electrical and electrochemical measurements as predictors of corrosion at the metal—organic coating interface. Progress in Organic Coatings, 7(1), 79-104.
[2] Walter, G. W. (1986). A critical review of the protection of metals by paints. Corrosion Science, 26(1), 27-38.
[3] Funke, W. (1997). Problems and progress in organic coatings science and technology. Progress in Organic coatings, 31(1-2), 5-9.
[4] Sørensen, P. A., Kiil, S., Dam-Johansen, K., & Weinell, C. E. (2009). Anticorrosive coatings: a review. Journal of coatings technology and research, 6(2), 135-176.
[5] Kendig, M., & Scully, J. (1990). Basic aspects of electrochemical impedance application for the life prediction of organic coatings on metals. Corrosion, 46(1), 22-29.
[6] Bonora, P. L., Deflorian, F., & Fedrizzi, L. (1996). Electrochemical impedance spectroscopy as a tool for investigating underpaint corrosion. Electrochimica acta, 41(7-8), 1073-1082.
[7] Deflorian, F., Fedrizzi, L., Rossi, S., & Bonora, P. L. (1999). Organic coating capacitance measurement by EIS: ideal and actual trends. Electrochimica Acta, 44(24), 4243-4249.
[8] Mansfeld, F. (1995). Use of electrochemical impedance spectroscopy for the study of corrosion protection by polymer coatings. Journal of applied electrochemistry, 25(3), 187-202.
[9] Bierwagen, G. P., He, L., Li, J., Ellingson, L., & Tallman, D. E. (2000). Studies of a new accelerated evaluation method for coating corrosion resistance—thermal cycling testing. Progress in organic coatings, 39(1), 67-78.
[10] Montemor, M. F. (2014). Functional and smart coatings for corrosion protection: A review of recent advances. Surface and Coatings Technology, 258, 17-37.
[11] Shi, X., Nguyen, T. A., Suo, Z., Liu, Y., & Avci, R. (2009). Effect of nanoparticles on the anticorrosion and mechanical properties of epoxy coating. Surface and Coatings Technology, 204(3), 237-245.
[12] Hanemann, T., & Szabó, D. V. (2010). Polymer-nanoparticle composites: from synthesis to modern applications. Materials, 3(6), 3468-3517.
[13] Bagherzadeh, M. R., & Mahdavi, F. (2007). Preparation of epoxy–clay nanocomposite and investigation on its anti-corrosive behavior in epoxy coating. Progress in Organic Coatings, 60(2), 117-120.

[14] Khun, N. W., Troconis, B. R., & Frankel, G. S. (2014). Effects of carbon nanotube content on adhesion strength and wear and corrosion resistance of epoxy composite coatings on AA2024-T3. Progress in Organic Coatings, 77(1), 72-80.
[15] Deyab, M. A., El-Shamy, O. A., Alghamdi, M. M., & El-Zahhar, A. A. (2024). Impact of Co3O4 nanoparticles on epoxy's mechanical and corrosion-resistance properties for carbon steel in seawater. Scientific Reports, 14(1), 3535.
[16] Hunter, R. J. (2013). Zeta potential in colloid science: principles and applications (Vol. 2). Academic press.
[17] Rammelt, U., & Reinhard, G. (1990). On the applicability of a constant phase element (CPE) to the estimation of roughness of solid metal electrodes. Electrochimica Acta, 35(6), 1045-1049.
[18] Ramezanzadeh, B., Attar, M. M., & Farzam, M. (2011). Effect of ZnO nanoparticles on the thermal and mechanical properties of epoxy-based nanocomposite. Journal of thermal analysis and calorimetry, 103(2), 731-739.
[19] Twite, R. L., & Bierwagen, G. P. (1998). Review of alternatives to chromate for corrosion protection of aluminum aerospace alloys. Progress in organic coatings, 33(2), 91-100.
[20] Zheludkevich, M. L., Shchukin, D. G., Yasakau, K. A., Möhwald, H., & Ferreira, M. G. (2007). Anticorrosion coatings with self-healing effect based on nanocontainers impregnated with corrosion inhibitor. Chemistry of Materials, 19(3), 402-411.
[21] Haddadi, S. A., SA, A. R., Mahdavian, M., & Arjmand, M. (2021). Epoxy nanocomposite coatings with enhanced dual active/barrier behavior containing graphene-based carbon hollow spheres as corrosion inhibitor nanoreservoirs. Corrosion Science, 185, 109428.
[22] American Society for Testing and Materials. (2019). Standard Practice for Operating Salt Spray (Fog) Apparatus (ASTM B117-19).
[23] ASTM International. (2023). Standard practice for operating salt spray (fog) apparatus (ASTM B117). ASTM International.
[24] Salmoria, G. V., Gindri, I. M., & Martins, W. F. Comparing Oxygen Plasma, Hydrogen Peroxide and Flame Treatments of Polyamide Tubes to Hydrophilic Coating Adhesion.